Chem Rev Lett 9 (2026) 254-268

Research Article

Chemical Review and Letters
journal homepage: www.chemrevlett.com
ISSN (online): 2645-4947 (print) 2676-7279

Analyzing the binding affinity of anti-cancer drug sunitinib with natural and synthetic cyclodextrins: A computational study of inclusion complex formation

Leila Hokmabady[1,*], Farhad Gholampour[1], Fatemeh Ravari[1]

[1]*Department of Chemistry, Faculty of Science, Payame Noor University (PNU), 19395-4697, Tehran, Iran.*

ARTICLE INFO

Article history:
Received 13 November 2025
Received in revised form 21 December 2025
Accepted 25 December 2025

Keywords:
Natural and modified cyclodextrins
Sunitinib
Drug delivery
Molecular docking
Molecular dynamics simulation

ABSTRACT

This study delves into the potential of six different natural cyclodextrins, including alpha-cyclodextrin, beta-cyclodextrin, and gamma-cyclodextrin, and modified CDs like Amino-BCD, methylated-BCD, and 2-hydroxypropyl-beta-cyclodextrin, in Sunitinib, a potent inhibitor of multiple tyrosine kinase receptors with significant antitumor effects. Computational techniques such as molecular docking and molecular dynamics simulation were employed in this exploration. The molecular docking results reveal that Sunitinib forms inclusion complexes with all six CDs, with the highest affinity observed with methylated-beta-cyclodextrin. RMSD analysis of MD simulation trajectories confirm the formation of stable complexes of Sunitinib with all six CDs. However, according to the distance analysis, it can be inferred that among all the natural and modified CDs, gamma-cyclodextrin and methylated-beta-cyclodextrin have the most dependable interaction complexes with Sunitinib. The reduced hydrogen bond formation with the solvent in inclusion complexes compared to free CDs indicates that Sunitinib displaces water molecules from the internal wall, highlighting the formation of hydrogen bonds between the CDs and Sunitinib and underscoring the potential of CDs for drug encapsulation. Interaction energy analysis emphasizes the significant role of van der Waals interactions in the encapsulation of Sunitinib within CDs and suggests that methylated-beta-cyclodextrin and beta-cyclodextrin are the optimal choices for the delivery of Sunitinib.

1. Introduction

Sunitinib (SUTENT®, SUT), with C22H27FN4O2 molecular formula (Scheme 1), is a powerful inhibitor of multiple tyrosine kinase receptors, including vascular endothelial growth factor, platelet-derived growth factor, stem cell factor, FMS-like tyrosine kinase 3, colony-stimulating factor 1, and RET proto-oncogene receptors [1]. This compound has been proven to have antitumor effects in metastatic renal cell carcinoma and imatinib-resistant metastatic gastrointestinal stromal tumor [2]. However, SUT may lead to various side effects such as weakness, vomiting, nausea, constipation, and diarrhea, bloody or black and tarry stools, swelling, tenderness, warmth, or redness of a leg, swelling of the feet or ankles, depression, dizziness or fainting [3] and hypothyroidism [4]. It is also known to cause hypothyroidism and is sensitive to light exposure [5]. Due to its low aqueous solubility and chemical instability in water, SUT has limited therapeutic benefits [6].

In order to address these issues, researchers have proposed exploring the use of carbohydrate-based macromolecules such as cyclodextrins (CDs) to improve the solubility and decrease the adverse effects of drugs. CDs are donut-shaped molecules composed of cyclic oligosaccharides of D-glucopyranose [7]. These molecules have a large central cavity that enhances their solubility and allows them to form inclusion complexes (ICs) with hydrophobic compounds like drugs, food ingredients, vitamins, and insoluble or poorly soluble substances [8]. Three types of natural CDs are alpha-cyclodextrin (ACD), beta-cyclodextrin (BCD), and gamma-cyclodextrin (GCD) with 6, 7 and 8 units, respectively. They possess a hydrophilic exterior and a hydrophobic interior cavity [9,10].

These cyclic molecules are a fascinating subject because of their inherent presence in nature and diverse biological functions, making them perfect for drug delivery purposes [11–14], food technology, the human diet [15], and agriculture industry [8]. Unaltered and

* Corresponding author E-mail: l.hokmabadi@pnu.ac.ir
https://doi.org/10.22034/crl.2025.559567.1733

modified BCDs are notable among CDs for their unique characteristics, including the optimal void volume and cost-effectiveness, which makes them particularly intriguing [11].

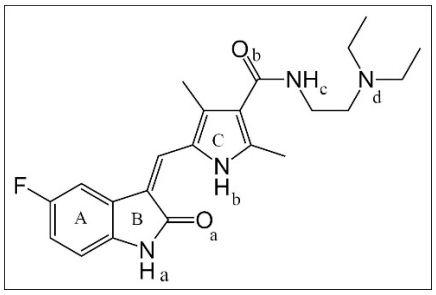

Scheme 1. Molecular structure of SUT

Modified BCDs, such as Amino-BCD (AMB) [16], random methylated-BCD (RMB) [17,18], and 2-hydroxypropyl-BCD (HPB) [10,19], are examples of modified BCDs that have been thoroughly investigated for their capacity to enhance the stability, solubility, pharmacokinetics, bioavailability, biocompatibility, and minimize adverse effects of active pharmaceutical ingredients [13,19].

The use of different carriers to deliver various drugs has been discovered to improve their solubility and absorption when taken orally [20–24]. Using this system, it is possible to speed up drug release and also control the drug by doctors. In recent years, a variety of novel nanocarrier systems have attracted increasing attention in drug delivery research. Among them, polymeric scaffolds containing sodium alginate microspheres, fullerene oxide nanocages, and chitosan–salicylic acid-based structures have been explored as promising platforms for the encapsulation and controlled release of pharmaceutical compounds [25-27].

We have previously investigated the behavior of other tyrosine kinase inhibitors such as nilotinib, crizotinib, and erlotinib with cyclodextrins [28-30]. Sunitinib has a distinct chemical structure, polarity distribution, and functional groups that lead to a different interaction mechanism and encapsulation pattern in cyclodextrin cavities. Yet, to date, there has been no comprehensive research examining the creation of inclusion complexes between CDs and SUT using computational methods. Therefore, this study represents a novel and necessary extension of our previous research. We undertook an extensive study to assess the molecular properties of the formation of inclusion complexes between natural CDs including ACD, BCD, and GCD and modified BCDs including HPB, RMB, and AMB (Scheme 2) with SUT through molecular docking and molecular dynamics (MD) investigations. The results of this research have the potential to aid in determining the effectiveness of these formulations as targeted drug delivery systems, with the aim of enhancing stability and reducing the adverse effects associated with cancer therapy.

2. Computational methods

2.1. Preparation of cyclodextrins and Sunitinib structures

The 3D molecular structure of SUT (PubChem CID: 5329102) was retrieved from the chemical compound library on the PubChem database website [31]. The initial structures of unmodified CDs, ACD (PDB ID: 1BTC) [32], BCD (PDB ID: 3CGT) [33], and GCD (PDB ID: 1D3C) [34]) were obtained from the RCSB database [35]. The 3D structures of AMB, HPB, and RMB were obtained by randomly substituting BCD using GaussView 5.0 software [36].

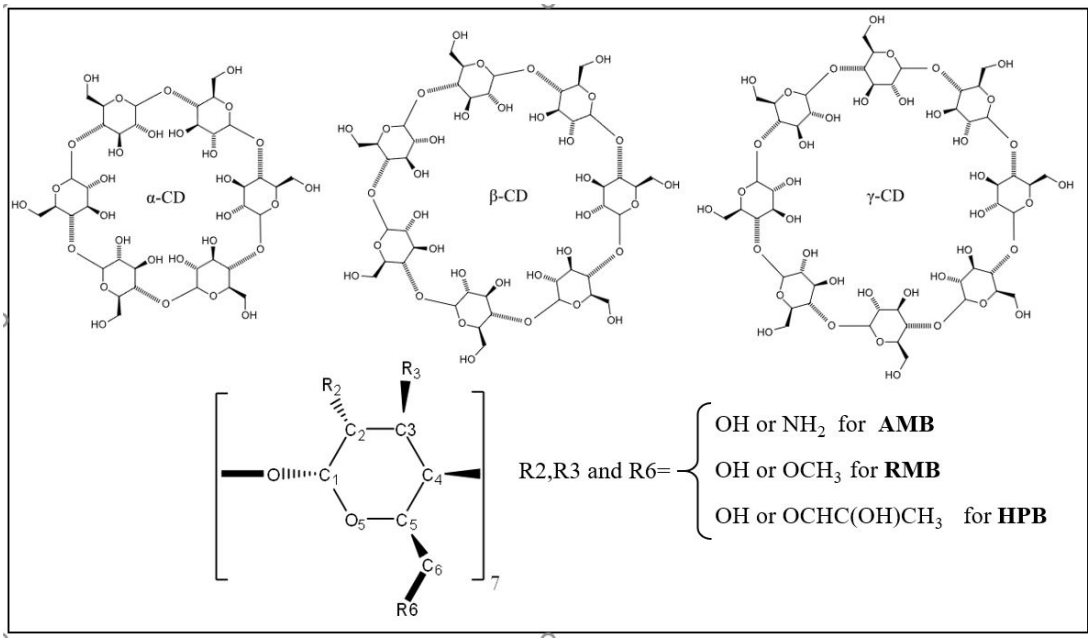

Scheme 2. Molecular structures of natural and modified CDs.

2.2. Molecular docking

Molecular docking is a computational technique utilized to predict how well a molecule will bind to its target macromolecule. It plays a crucial role in drug delivery research and can greatly impact the advancement of new and improved therapies. Molecular docking is instrumental in identifying any potential side effects or toxicity of drugs, determining optimal dosages, and screening large compound libraries to assess their binding potential [37].

AutoDock 4.2.6 software was utilized for conducting molecular docking experiments [38]. Initially, to prepare coordinate files for all CDs and SUT, PDBQT files were generated.

The CDs were treated as rigid, while SUT was considered flexible, with all torsional bonds allowed to rotate freely. The grid point spacing was set to 0.375 Å, and the box size to 40 × 40 × 40 Å3 points. The Lamarckian Genetic Algorithm (LGA) was employed with default parameters, and 200 docking runs were conducted with 25,000,000 energy evaluations per run. Binding energy was calculated using ranking functions, and conformations within each cluster were sorted based on their binding energy. The optimal docking pose was chosen based on the structure with the lowest binding free energy in the most populated cluster [39].

2.3. Molecular dynamics simulation

Molecular dynamics simulations can be employed to design CD-based drug delivery systems by predicting the behavior of the complexes over time [40]. While molecular docking is able to assess the binding energy and orientation of SUT within the cavity by treating the receptor as rigid, it fails to capture the dynamic nature of the binding process [41].

In this context, recent studies have successfully demonstrated the effectiveness of MD simulations in elucidating structural and electronic properties of complex molecular systems, highlighting their crucial role in understanding molecular interactions in solution and condensed phases. In this study, the optimal docking poses were selected to serve as the starting structures for MD calculations. The systems ACD, BCD, GCD, AMB, HPB, and RMB were all included in a box of SPC/E water molecules. Table 1 presents the number of water molecules and the size of a space-filling cubic box for the systems containing free CDs and CD:SUT ICs. The MD simulations for each system were conducted using GROMACS 2018.8 software [42] and the Charmm36 force field [43].

Periodic boundary conditions were applied to all three-dimensional spaces of both free and complex CDs. The force field parameters for SUT and CDs were obtained from the CGenFF web server [44]. After performing energy minimization using the steepest descent algorithm, the system was equilibrated and relaxed.

Following this, the system was heated to 310 K using a V-rescale thermostat for a 10 ns simulation time in the canonical ensemble (NVT) [45,46]. The system pressure was maintained at a constant 1 bar for a duration of 10 ns using the Parrinello-Rahman barostat in conjunction with an isothermal-isobaric (NPT) ensemble [47]. The particle mesh Ewald (PME) method was used to consider the long-range electrostatic forces, utilizing a cutoff of 12 Å [48].

The van der Waals interactions were computed using the Lennard-Jones potential with a cutoff distance of 12 Å and the Lincs algorithm was applied during the calculation [49]. Finally, a 300 ns production run with constant temperature and pressure was conducted using a 2-fs time step and the leapfrog algorithm.

2.4. DFT analysis

The structures of the SUN drug, native and modified CDs, and inclusion complexes were optimised using M06-2X [50] with the 6-31G basis set [51], as implemented in the Gaussian 09 program package [52] in the aqueous solution. All geometry optimizations were performed using the default convergence criteria in Gaussian 09.

The optimization was considered converged when the maximum force was below 0.00045 a.u., RMS force below 0.00030 a.u., maximum displacement below 0.0018 Å, and RMS displacement below 0.0012 Å. The M06 set of meta-hybrid functionals includes an empirical fitting of its parameters that allows an increased response to dispersion forces.

Table 1. The dimensions of a space-filling cubic simulation box and the number of water molecules

Systems	Number of water molecules	Dimensions of cubic box $(nm)^3$	Systems	Number of water molecules	Dimensions of cubic box $(nm)^3$
ACD	1169	3.34086	ACD: SUT IC	1288	3.46714
BCD	1380	3.56146	BCD: SUT IC	1621	3.78594
GCD	1631	3.77450	GCD: SUT IC	1620	3.77581
HPB	2325	4.18165	HPB: SUT IC	2238	4.16047
AMB	1390	3.57374	AMB: SUT IC	1623	3.79437
RMB	1437	3.61947	RMB: SUT IC	1652	3.88940

This level of theory is particularly suitable for modeling host–guest systems and drug–cyclodextrin inclusion complexes dominated by noncovalent interactions. DFT-D3, an extended framework with newly implemented Grimme corrections, was applied to all DFT calculations [53].

The binding energy (E_{bind}) for the encapsulated SUN drug into CD was obtained as follows:

$$Ebind = ESUN\text{-}CD - (ESUN + ECD) \quad (1)$$

The chemical reactivity and kinetic stability of the inclusion complexes were defined using the energies of HOMO and LUMO molecular orbitals [54,55].

3. Results and Discussion

3.1. Molecular docking analysis

This study utilized molecular docking to evaluate the insertion of SUT into both natural and substituted CD cavities. The findings of the molecular docking analysis, as shown in Figures 1 and 2 and outlined in Table 2, demonstrate the optimal binding interactions between CDs and SUT, including the free binding energy ($\Delta G_{binding}$), inhibition constant (Ki), and the number of hydrogen bonds formed in these ICs.

In the examination of the ACD:SUT IC, the formation of a lone hydrogen bond between ACD and SUT was observed. This bond is depicted between the NHa group of SUT and the -OH group at the C-6 position of ACD. Furthermore, Figure 2 demonstrates that SUT is inserted into the ACD cavity, with rings A and B located on the narrower side and the aliphatic chain on the wider side of the cavity.

Analysis of the molecular docking of BCD:SUT IC indicated the presence of three hydrogen bonds. One bond formed between the NHa group of SUT and O4 of BCD, while the other two bonds formed between the NHc and Nd groups in the aliphatic chain of SUT and the -OH group at the C-2 position of BCD. In Figure 2, it can be observed that the ring C and the aromatic chain of SUT are situated in the broader and narrower sides of the BCD cavity, respectively. In the GCD: SUT complex, there are two hydrogen bonds created between the NHa and O2 of GCD, and between the NHc in the aliphatic chain of SUT and the -OH group at C-6 in GCD. In addition, SUT is partially positioned inside the GCD cavity. Similar to the ACD: SUT and BCD: SUT complexes, it can be seen that the ring C and the aromatic chain of SUT are situated in the wider and narrower sides of the GCD cavity, respectively. The molecular docking analysis of RMB and SUT indicated the formation of two hydrogen bonds between NHa and NHc groups in SUT, and O6 and O5 atoms in RMB. Moreover, SUT was observed to be positioned in the RMB cavity in a twisted manner, partially inserted into the wider side. In the same vein, the molecular docking analysis of HPB and SUT revealed the formation of a lone hydrogen bond between NHa group of SUT and the O atom at the C-1 position in HPB. When SUT was inserted into HPB's cavity, it adopted a distinct orientation, with the aliphatic chain positioned on the wider side and ring-A on the narrower side. In the AMB and SUT case, molecular docking analysis revealed three hydrogen bonds between NHa, NHc, and Nd groups of SUT and the O atom at the C-1 position, O2, and O3 atoms of AMB. The positioning of the SUT in the AMB cavity indicated insertion, with the aliphatic chain on the wider side and rings A and B on the thinner side. The comparison of the binding energy and inhibition constant for the six ICs revealed that the affinity of the SUT with CDs followed the order: RMB: SUT > HPB: SUT > GCD: SUT > BCD: SUT > ACD: SUT > AMB: SUT. Overall, all CDs form stable ICs with SUT, and both van der Waals and hydrogen bond interactions are important in their formation.

Table 2. The free binding energies ($\Delta G_{binding}$) and inhibition constants (Ki) for the best docking conformations.

Inclusion Complex	$\Delta G_{binding}$ (kcal/mol)	K_i(μM)
ACD: SUT IC	-5.27	137.9
BCD: SUT IC	-5.74	61.95
GCD: SUT IC	-5.85	51.84
RMB: SUT IC	-6.62	14.13
AMB: SUT IC	-5.18	160.67
HPB: SUT IC	-6.60	14.64

3.2. Molecular dynamics simulation

Computational methods were used to conduct MD simulations to study the free CDs and the ICs. These simulations were utilized to model the behavior of the CD molecules and their associated guest molecules over time, providing insights into the stability and dynamics of the complex, as well as the interactions between the host and guest molecules.

3.2.1. Structural analysis of free CDs

Prior to conducting molecular docking, MD simulations were performed on unmodified and modified CDs in water for 300 ns. The snapshots of the CDs at 0, 100, 200, and 300 ns are shown in Figure 3. The ACD structure remained stable at 0 and 100 ns but became unstable after 200 ns, closing on one side. The BCD structure remained constant throughout the simulation, while GCD underwent conformational changes in its glucopyranoside units after 200 ns. Snapshot analysis also included modified cyclodextrin structures. Methyl and amine functional groups exhibited some flexibility, with the AMB and RMB conformations remaining partially unchanged. In contrast, HPB with hydroxy-propyl groups showed flexibility and intramolecular hydrogen bond formation, leading to conformation changes after 100 ns and cavity closure after 200 ns of simulation.

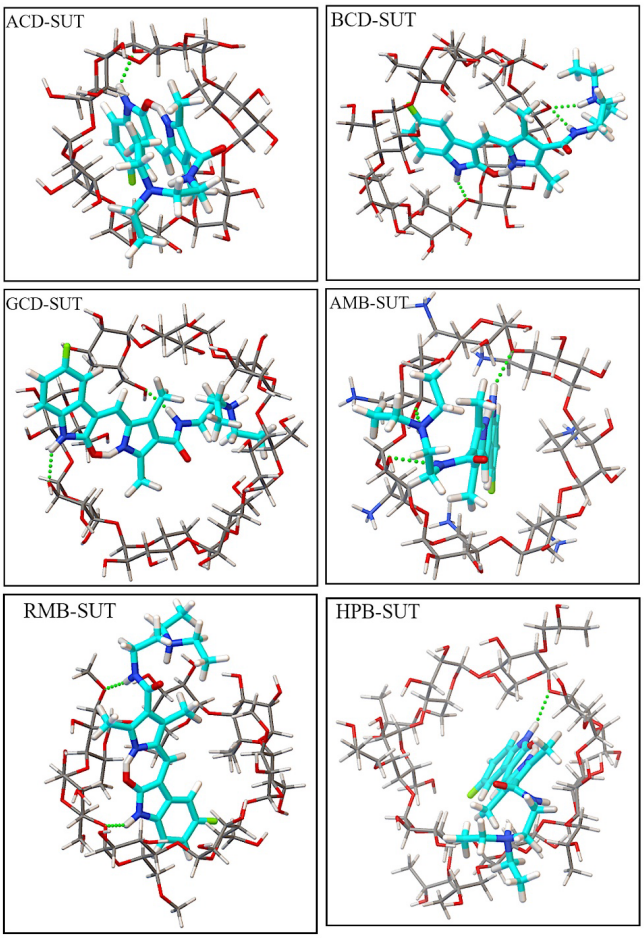

Fig. 1. The best docking pose for the SUT:CDs ICs.

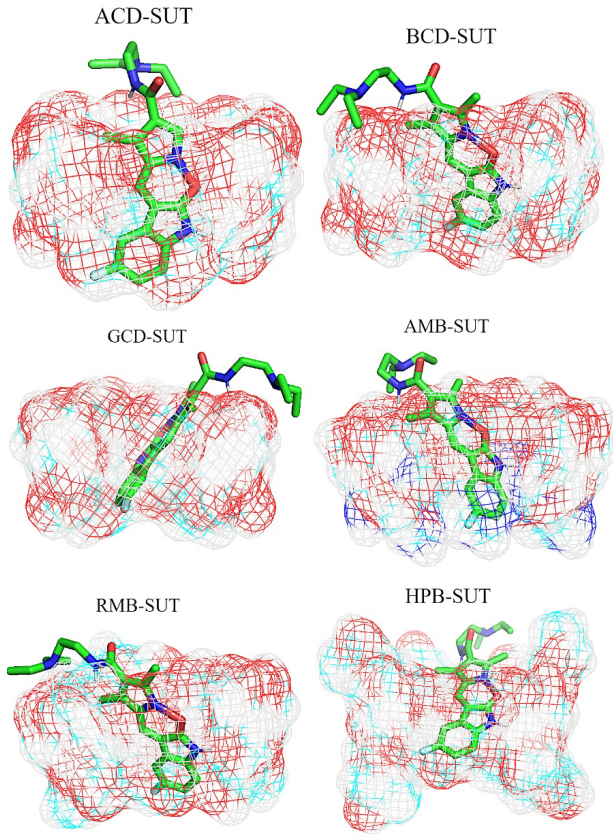

Fig. 2. 3D presentation of SUT insertion in the CDs cavity (the best docking pose), prepared by pymol progarm.

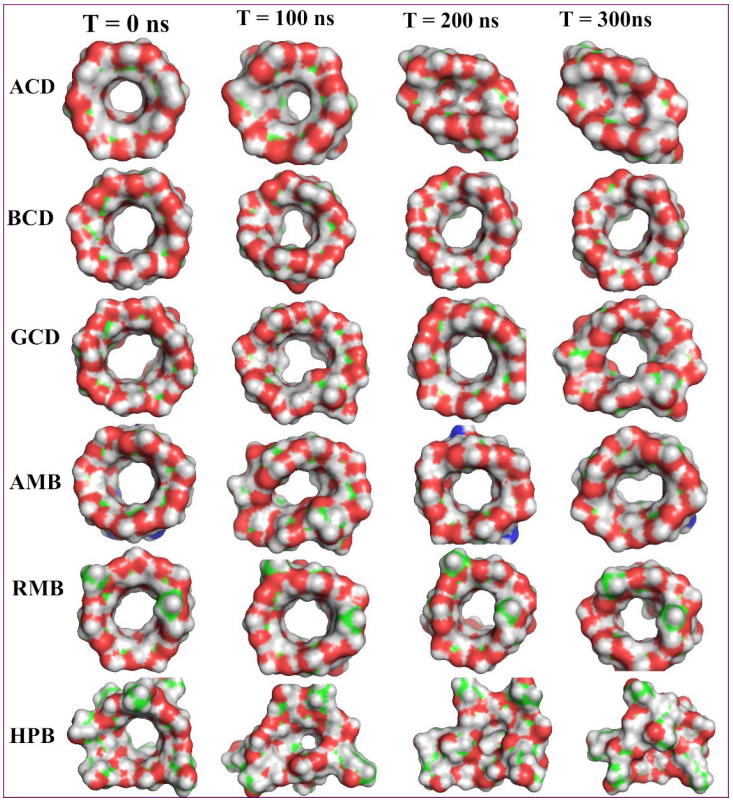

Fig. 3. The snapshots of the free CDs in water solution every 100 ns.

3.2.2. Root mean square deviation (RMSD)

The RMSD analysis assesses the variation in atomic positions within a simulated complex compared to a reference structure. It is utilized for stability evaluation, equilibration determination and conformational analysis in MD simulations. In this study, the RMSD analysis was used to compare the structures of natural and substituted CDs in both their free and complex forms over a 300 ns simulation period. The results, as shown in Figure 4, revealed that in the free ACD system, a small gap of approximately 0.08 nm was observed at 150 ns, whereas in the ACD:SUT IC system, similar gaps were seen at 30, 150, and 250 ns. However, the free and complex ACD systems converged in the final 50 ns of the simulation.

The free BCD system exhibited equilibrium in RMSD from 0 to 250 ns, with a shift occurring after 250 ns. In contrast, the BCD:SUT IC system maintained balance throughout the entire simulation period. Similarly, the free GCD system displayed a small shift at approximately 90 and 170 ns, while the GCD:SUT IC system remained stable throughout the simulation time. The RMSD analysis for the free and complex forms of RMB and HPB revealed that these systems reached equilibrium after about 200 ns simulation, with some minor fluctuations observed.

For free AMB system two small gap were observed at 25 and 140 ns and both free AMB and AMB:SUT IC systems are in equilibrium state in the last 100 ns . Overall, as demonstrated in Table 3 the results indicated that with the exception of ACD the complex states of CDs showed greater stability than their free states, with smaller mean RMSD.

3.2.3. Distance analysis

In MD simulations of CD:drug complexes, it is crucial to conduct distance analysis between the center of mass (COM) of CDs and drugs. This analysis is indispensable for evaluating the stability of the complex assessing the interaction between CDs and the drug, and predicting binding affinity in aqueous solutions [56]. On the other hand, the dynamics of the insertion of the drugs into the CD cavities can be studied by evaluating the distance between the COM of the drug and CDs throughout the simulation [19,57]. Figure 5 demonstrates large fluctuations in the distance between the COMs of SUT and ACD at 25, 75, and 110 to 130 ns of simulation time. This could be attributed to the small size of the ACD cavity compared to the size of the anticancer drug SUT. Similar fluctuations were observed in the COMs of BCD and SUT distances at 75 to 100 ns, 150 to 175 ns, and around 300 ns. Interestingly, no fluctuations were observed in the distances between the COMs of GCD and SUT after the formation of IC. In the RMB: SUT IC, fluctuations were seen in the distance between COMs in 210-230 ns, 240-250 ns, and approximately 300 ns, while the distance remained constant for the rest of the simulation time.

Fluctuations were also observed in the COMs of AMB and SUT distances at various time intervals. The distance between the COMs of the SUT and HPB showed

continuous fluctuations, possibly indicating the drug's release from the cavity and contributing to the instability of this IC compared to other ICs. Overall, the distance analysis suggests that among natural and modified CDs, GCD and RMB form the most consistent interaction complexes with SUT

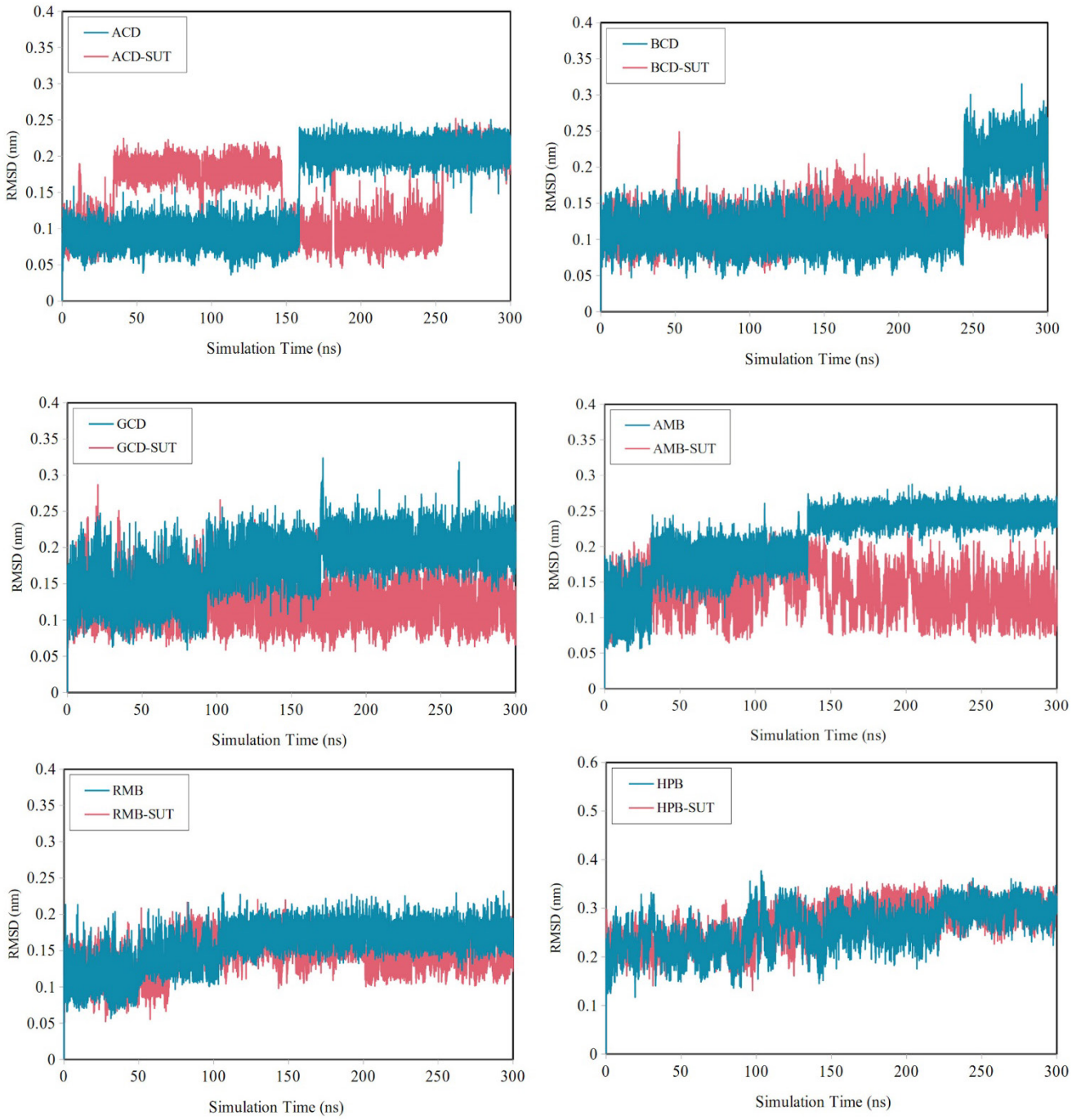

Fig. 4. RMSD of free CDs and IC states for CDs with SUT during the 300 ns simulation time.

Table 3. The mean RMSD (nm) of CDs in free and in complex with SUT in last 30 ns.

Free system	Mean RMSD (nm)	IC system	Mean RMSD (nm)
ACD	0.208±0.013	ACD: SUT IC	0.214±0.011
BCD	0.225±0.021	BCD: SUT IC	0.142±0.016
GCD	0.202±0.019	GCD: SUT IC	0.119±0.029
AMB	0.245±0.009	AMB: SUT IC	0.127±0.025
RMB	0.174±0.014	RMB: SUT IC	0.138±0.016
HPB	0.298±0.020	HPB: SUT IC	0.297±0.018

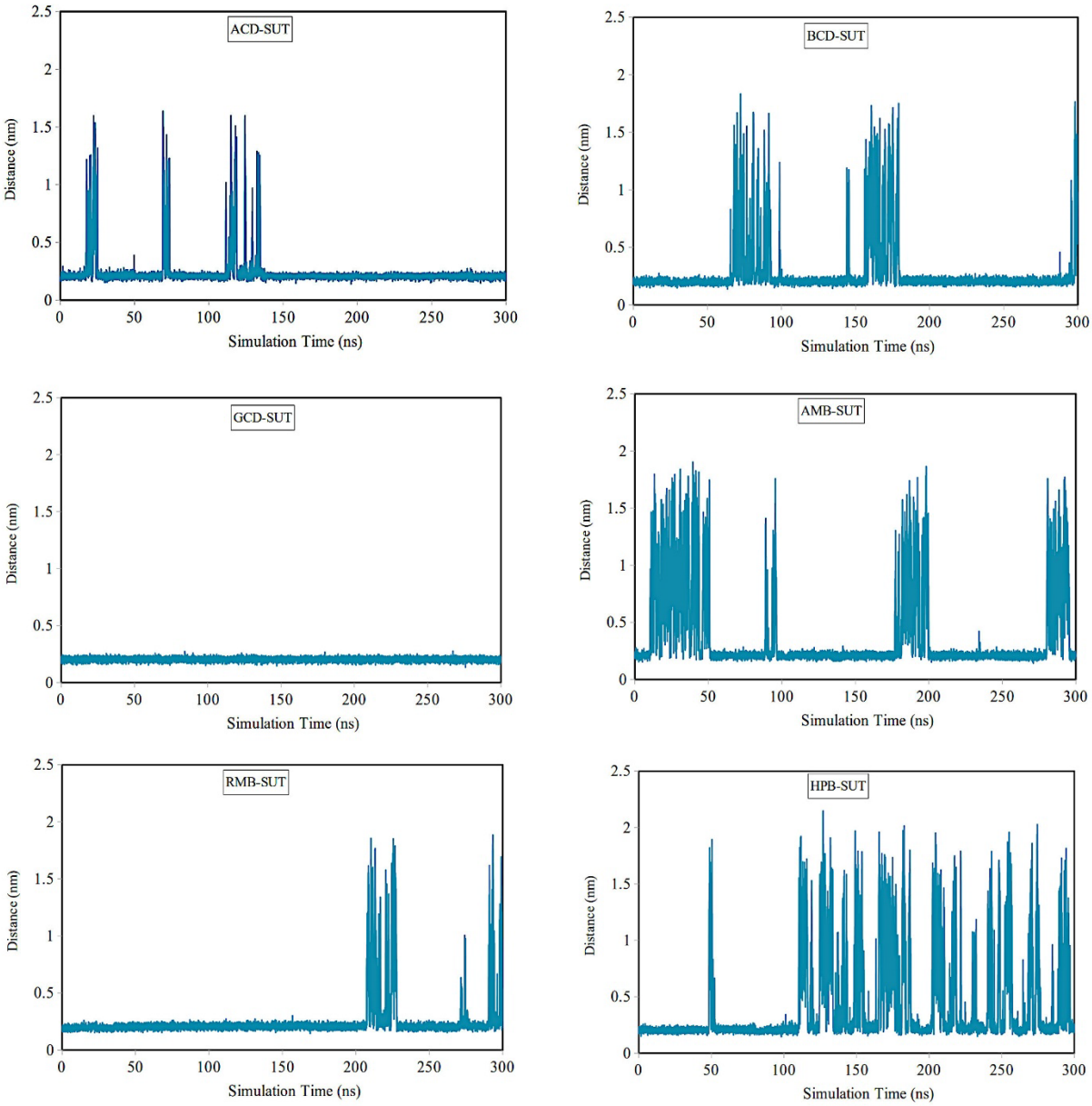

Fig. 5. The distance plots between COM of the SUT and the CDs during the whole simulation time.

3.2.4. The radial distribution function analysis

RDF analysis offers valuable insights into intermolecular interactions, helps validate the results of the MD simulations and improves the comprehension of the interactions between CDs and drugs [57]. As shown in Figure 6, the RDF of all natural and substituted CDs within the ICs with a cutoff of 1.8 nm was calculated based on the water molecules surrounding the oxygen atoms of the glucopyranose units. This provided insightful information on the distribution of water molecules inside and around the CD cavities [58,59]. This information results from the flexibility of the glucopyranose units and the hydrogen bonds formed between the CDs and water molecules in their surroundings.

In Figure 6, six RDF curves show how water molecules are distributed around the O3 atom in both free and complex states of CDs. The two peaks in each CD curve indicate the presence of water molecules interacting with the O3 atom of unmodified or modified CDs in both their free and complex forms. The peaks between 0.18 to 0.22 nm and 0.22 to 0.4 nm suggest hydrogen bonding interactions, with the highest intensities corresponding to water molecules in the outer cavity of the CDs, possibly due to hydrogen bonds forming between water molecules and the O3 atom of the CDs. In the complex state, the peak intensities were slightly lower than in the free CDs, indicating that water molecules had moved out of the CD cavities to make room for the SUT molecule.

The decrease in peak intensity was more significant in complex RMB compared to other CDs, suggesting that stable ICs form between SUT and this modified BCD. Molecular docking and distance analyses confirmed this result.

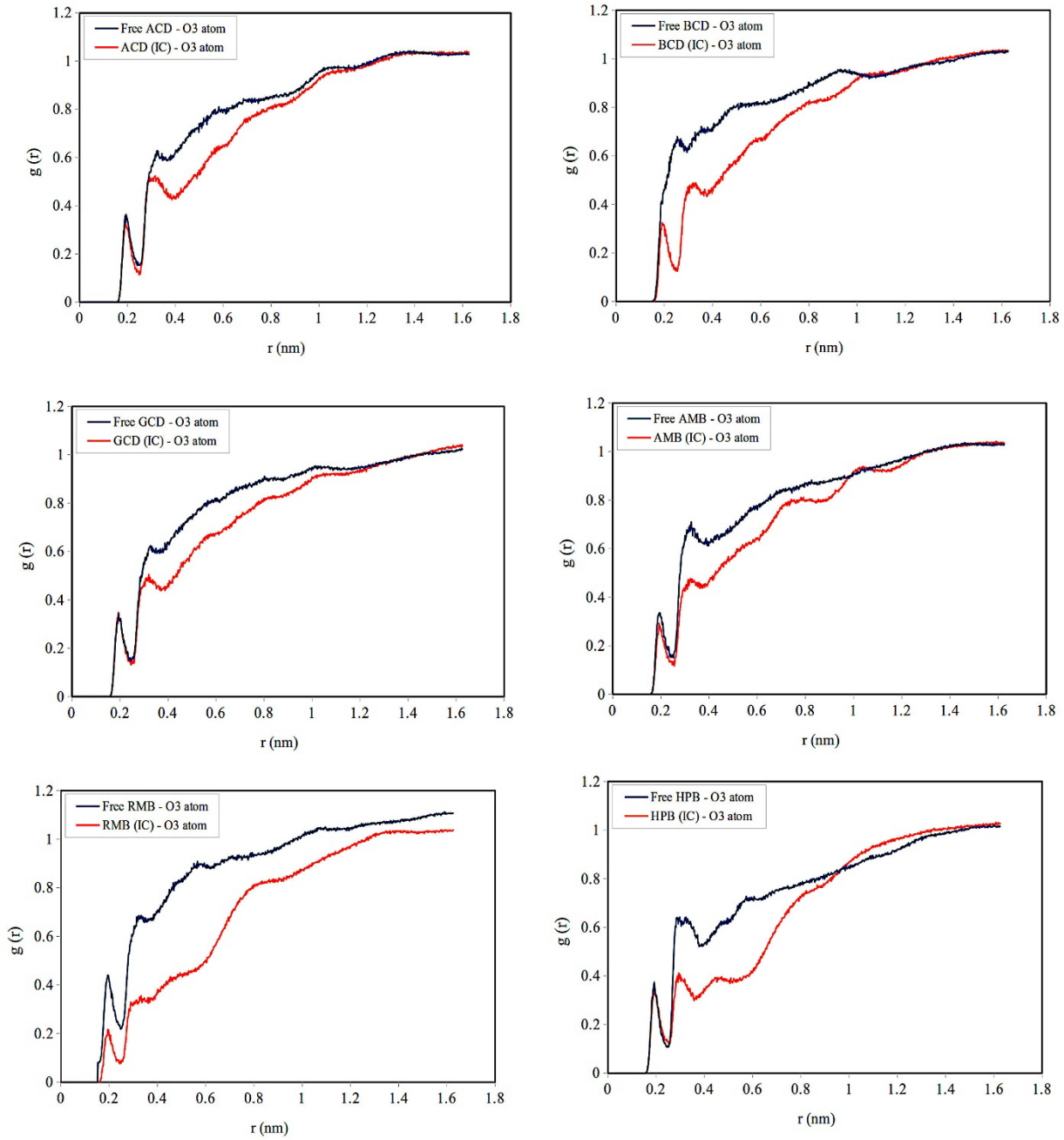

Fig. 6. The RDF plots for O3 atom of free and complex CDs during the 300 ns simulation time

3.2.5. Hydrogen bond analysis

Analysis of hydrogen bond is essential in the MD simulations to study the interactions between receptors and drug molecules. It helps to determine the strength and specificity of binding between two molecules, providing insights into their stability. Hydrogen bonds with water molecules also affect drug-receptor interactions, influencing drug solubility and transport in biological systems. Studying these interactions sheds light on how solvent molecules impact the binding affinity and stability of these complexes, crucial for understanding drug behavior in biological environments [58,60]. A hydrogen bond is established when the distance between the donor and acceptor is shorter than 0.35 nm and the angle between them is less than 30°.

The 0.35 nm distance aligns with the primary hydration shell of water molecules [61].

This study analyzed the number of hydrogen bonds formed between CDs and SUT, as well as between CDs and the solvent, to assess structural stability over a 300 ns simulation period. The research results indicate that intermolecular hydrogen bonds are essential for the stability of all ICs. A maximum of three hydrogen bonds form between ACD and SUT, while the other CDs can form up to five hydrogen bonds with SUT. Differences in the number of hydrogen bonds between SUT and ICs - especially in HPB- suggest increased flexibility of SUT within the cavity (Figure 7).

Figure 8 illustrates the time-dependent formation of hydrogen bonds between CDs in their free form and

inclusion complex with the solvent molecules.

The average number of hydrogen bonds formed between free CDs and the solvent is higher compared to complex CDs, likely due to the exposure of both internal and external surfaces of free CDs to the solvent. In contrast, the insertion of the SUT molecule displaces water from the internal wall of the complex CDs, reducing the solvent-accessible surface on the complex CDs.

Table 4 shows that the average number of hydrogen bonds between natural CDs and the solvent follows the order GCD > BCD > ACD, based on the size of the CDs with 6, 7, and 8 α-D-glucopyranoside units, respectively. The modified BCDs follow the order HPB > RMB > AMB, which can be attributed to the functional groups present on the modified CDs.

Table 4. Average number of hydrogen bonds between CDs (Free)/solvent and CDs (IC)/solvent during the last 30 ns simulation time.

System	CDs: Solvent	System	CDs: Solvent
ACD	26.695±3.234	ACD: SUT IC	23.416±3.225
BCD	31.274±3.467	BCD: SUT IC	29.058±3.500
GCD	36.850±3.888	GCD: SUT IC	31.757±3.482
RMB	28.707±3.267	RMB: SUT IC	25.518±3.241
AMB	30.721±3.784	AMB: SUT IC	26.908±3.161
HPB	39.564±3.987	HPB: SUT IC	37.819±4.379

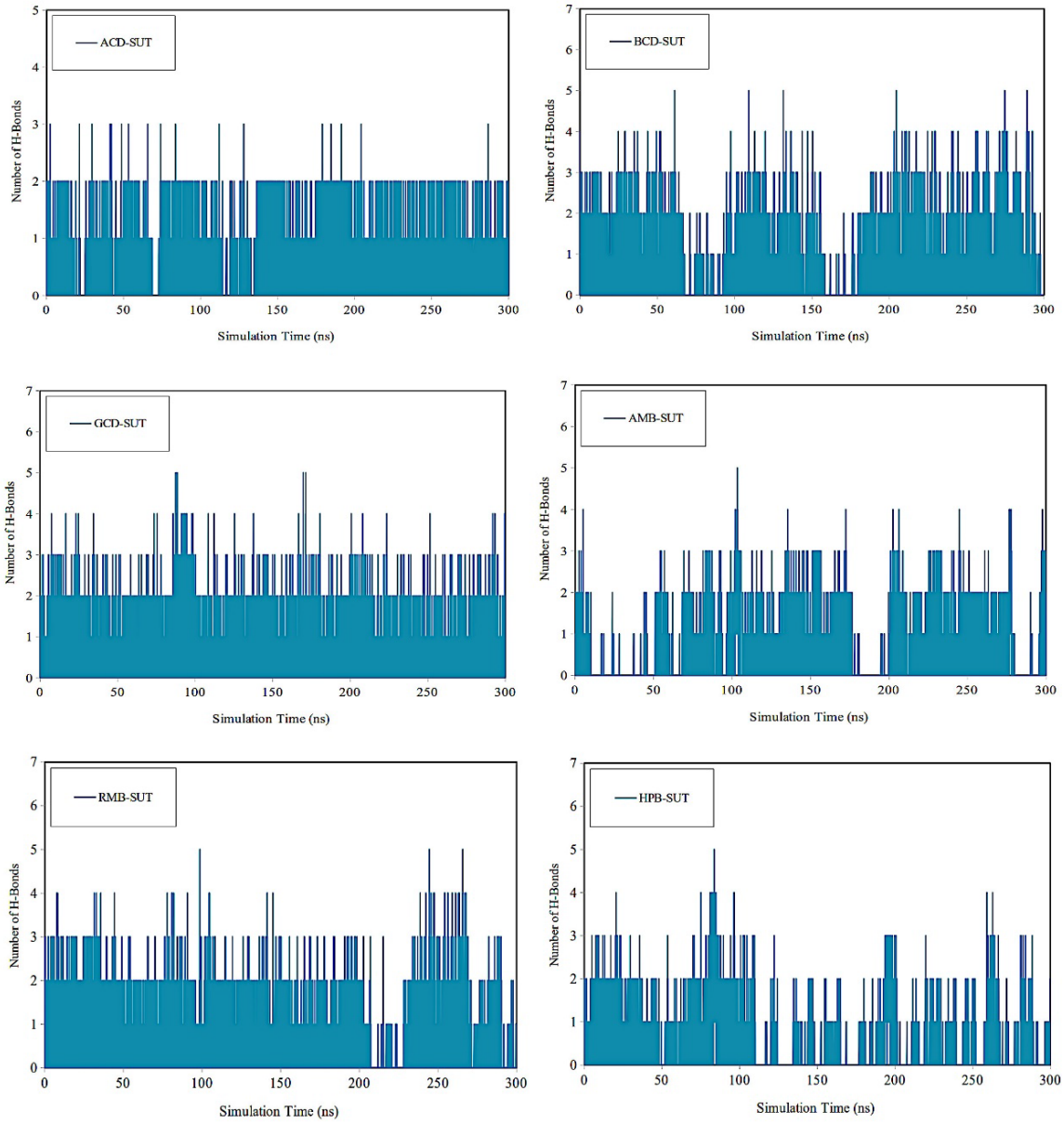

Fig. 7. The number of hydrogen bonds between CDs and SUT during the 300 ns simulation time

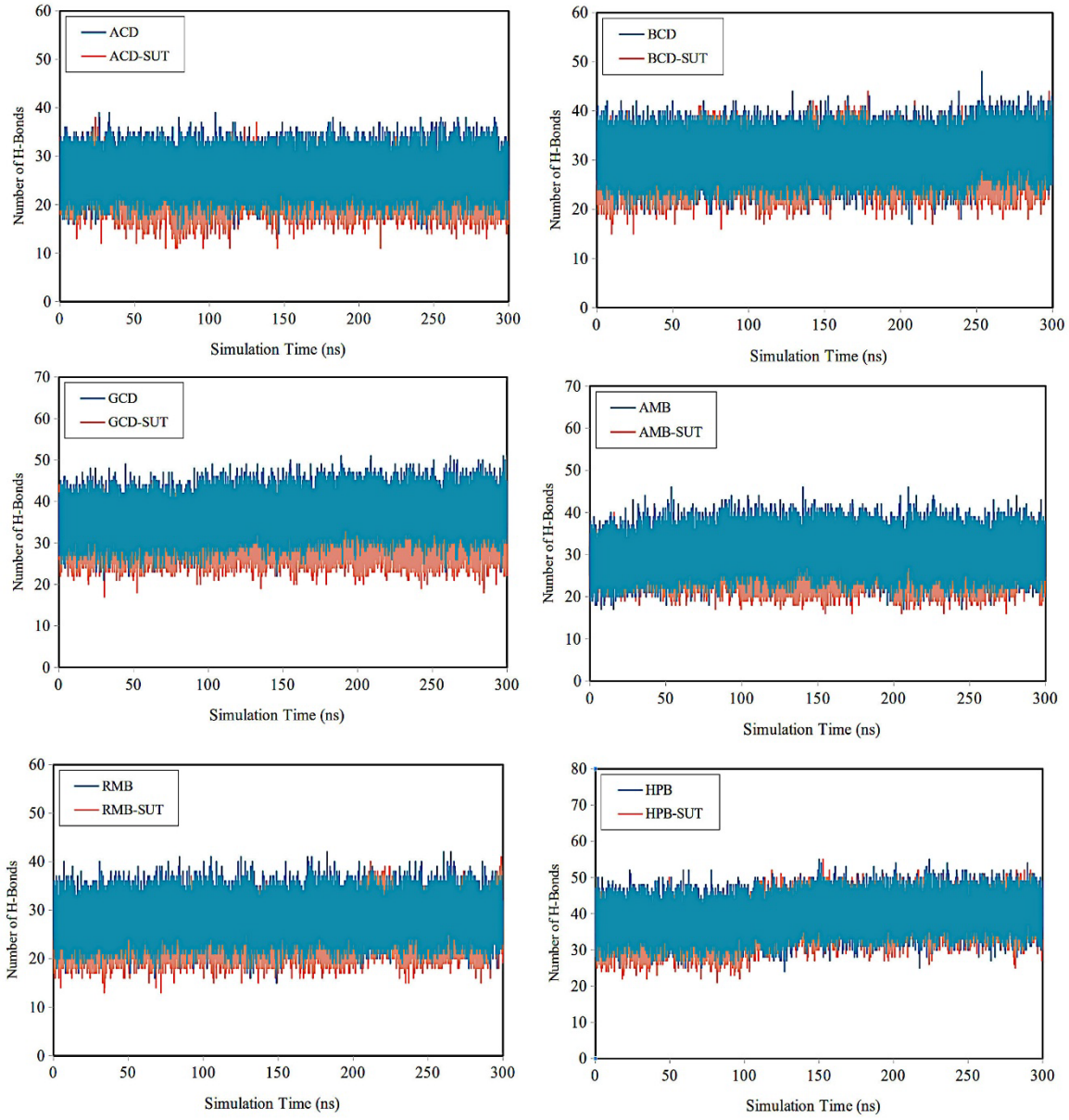

Fig. 8. The variation of hydrogen bonds for CDs (Free)/solvent and CDs (IC)/solvent during the 300 ns simulation time.

3.2.6. The interaction energy analysis

During the MD simulation, interactions between molecules were assessed using the Coulomb potential for electrostatic forces and the Lennard–Jones potential (LJ) for van der Waals interactions. Figure 9 indicates that all ICs consistently showed higher van der Waals interaction energies compared to electrostatic energies, highlighting the significant role of van der Waals interactions in the encapsulation of SUT within CDs. The data from the figure reveal the van der Waals interaction energy ranking for SUT with CDs as follows: GCD > RMB > BCD > ACD > AMB > HPB. Additionally, the comparison of electrostatic energies for the six ICs shows that the affinity of SUT with CDs is in the order: BCD > RMB > GCD > AMB > HPB > ACD.

The results indicate that BCD and GCD among natural CDs, and RMB among modified CDs, exhibit the highest van der Waals and electrostatic interaction energies, suggesting a strong binding affinity with SUT.

3.3. DFT analysis

Recent DFT-based studies have demonstrated the effectiveness of computational approaches in elucidating drug–nanocarrier interactions and evaluating the stability and binding mechanisms of anticancer drug delivery systems, highlighting the importance of such methods prior to experimental investigations [62-64]. To determine the most stable structure of SUN and native and modified CDs, all these monomers were initially fully optimised at the M06-2X/6-31G level of theory (Fig. 1 Supp.). The equilibrium structure of inclusion complexes derived from molecular dynamics simulations was utilized to assess the binding energy through DFT-D3 methods, and the results were provided in (Fig. 2 Supp.). As shown in this figure, the drug molecule was situated within the cyclodextrin cavity. The binding

energies were calculated using Formula (1) and reported in Table 5. The negative E_{bind} values for all inclusion complexes, generally caused by strong interactions between SUN and CDs, indicate that the insertion of SUN into CDs was an exothermic process. Generally, the conformation with a higher negative E_{bind} is considered more stable [65].

Herein, the AMB-SUN inclusion complexes displayed the most negative E_{bind} (-259.376 kJ/mol), indicating that AMB had stronger attractive forces for SUN compared to other types of CDs. The calculated dipole moment (μ_0) values for CDs and inclusion complex are listed in Table 5. The dipole moment value of the SUN drug is 5.576 Debye. These results indicate a considerable increase in the solubility of the inclusion complexes in comparison to free drug and cyclodextrins except in GCD. According to the results of the dipole moment, AMB-SUN inclusion complex shows the highest solubility. The HOMO–LUMO energy gap (ΔEgap) has a significant impact on the chemical reactivity and kinetic stability of a molecule. The energies of the HOMO (εHOMO) and LUMO (εLUMO) define the ionization energy and electron affinity, respectively, which were utilized to calculate the chemical reactivity descriptors for each inclusion complex and isolated components (SUN and CDs).

If the ΔEgap is smaller, less energy is required for an electron to jump from the HOMO to the LUMO. This is due to the energetic favorability of electron transfer between the HOMO (occupied) orbital and the LUMO (unoccupied) orbital. Therefore, a molecule with a high ΔEgap will have decreased chemical reactivity and improved chemical kinetic stability. The following equations were used to determine the chemical reactivity descriptors for the inclusion complexes and individual components (SUN and CDs) in water, including chemical potential (μ), electrophilicity index (ω), and chemical hardness (η).

$$\mu=(\varepsilon HOMO+\varepsilon LUMO)/2 \quad (2)$$

$$\eta=(\varepsilon LUMO-\varepsilon HOMO)/2 \quad (3)$$

$$\omega=\mu 2/2\eta \quad (4)$$

ACD–SUN has higher ω values, a measure of the compound's ability to receive electrons, indicating that they are more electrophilic.

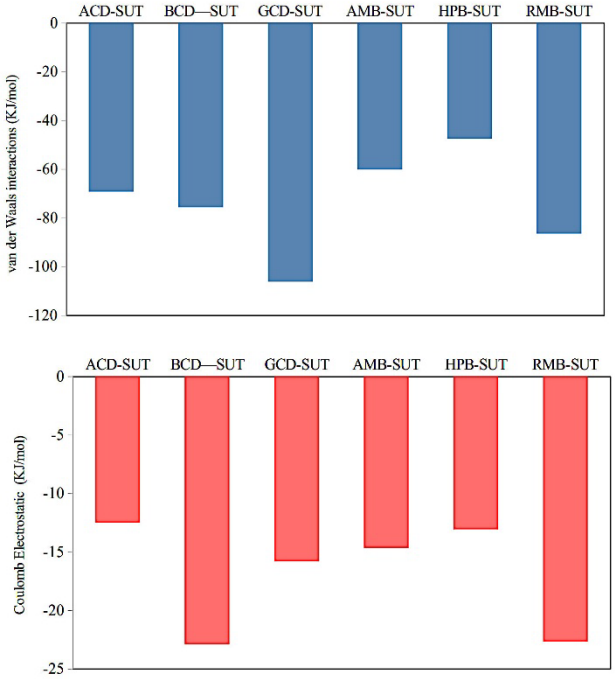

Fig. 9. The average Columbic and van der Waals energy of CDs with SUT during the last 30 ns.

Table 5. The binding energy (E_{bind}) in kJ.mol^{-1}, dipole moments (μ^0) in Debye, Chemical potential (μ), chemical hardness (η), and electrophilicity (ω) calculated for SUN-CD inclusion complexes in eV unit.

		μ^0						
	E_{bin}	**Free CD**	**IC**	**HOMO**	**LUMO**	**μ**	***η***	***ω***
ACD-SUN	-151.016	6.710	8.729	-0.251	-0.062	-0.157	0.095	0.129
BCD-SUN	-214.250	8.318	13.248	-0.245	-0.054	-0.150	0.095	0.118
GCD-SUN	-175.993	10.098	5.365	-0.237	-0.061	-0.149	0.088	0.126
AMB-SUN	-259.377	12.185	14.119	-0.241	-0.050	-0.146	0.095	0.111
RMB-SUN	-220.616	3.109	6.861	-0.248	-0.058	-0.153	0.095	0.123
HPB-SUN	-210.354	13.413	13.562	-0.245	-0.057	-0.151	0.094	0.121

4. Conclusion

In summary, our study showcased the potential of six different CDs in formulating SUT, an anticancer drug, using computational techniques like molecular docking and MD simulations. The docking results revealed that SUT formed inclusion complexes with all CDs, with the highest affinity observed with RMB and the lowest with AMB. Additionally, MD simulation unveiled distinct characteristics of the CDs, including the closure of the thinner side of ACD and HPB, and the flexibility of the hydroxy propyl groups in HPB. Based on the distance analysis, GCD and RMB have the most stable interaction complexes with SUT among the natural and modified CDs. The fluctuation in the distance between the centers of mass of SUT and HPB suggested that drug may be release from the CD cavity.

In the IC state of the CDs, the RDF peak intensities were lower than in free CDs, and the average number of hydrogen bonds formed with the solvent was lower compared to free CDs, indicating the replacement of water molecules within the CD cavities with SUT, underscoring the potential of CDs as a promising medium for this drug encapsulation. The results of the interaction energy analysis highlighted that among the modified CDs, RMB, and among the natural CDs, BCD and GCD, are the optimal choices for SUT, with the potential to enhance the stability, water solubility, and bioavailability of this drug. Overall, these findings provide valuable insights into drug formulation and delivery, paving the way for the development of more effective and safe anticancer treatments. Our research introduces new possibilities for improving the efficacy and safety of cancer therapies through innovative drug delivery methods utilizing CDs.

Future studies may focus on extending this computational approach to other anticancer drugs and cyclodextrin derivatives, as well as validating the predicted stability and solubility enhancements through experimental investigations

Supplementary files

Supplementary file 1.

References

[1] C. Le Tourneau, E. Raymond, S. Faivre, Sunitinib: A novel tyrosine kinase inhibitor. A brief review of its therapeutic potential in the treatment of renal carcinoma and gastrointestinal stromal tumors (GIST). *Ther. Clin. Risk Manag.*, 3 (2007) 341–348. https://doi.org/10.2147/tcrm.2007.3.2.341.

[2] M.C. Etienne-Grimaldi, N. Renee, H. Izzedine, et al., A routine feasible HPLC analysis for the anti-angiogenic tyrosine kinase inhibitor, sunitinib, and its main metabolite, SU12662, in plasma. *J. Chromatogr. B*, 877 (2009) 3757–3761. https://doi.org/10.1016/j.jchromb.2009.09.011.

[3] J.M.G. Larkin, T. Eisen, Kinase inhibitors in the treatment of renal cell carcinoma. *Crit. Rev. Oncol. Hematol.*, 60 (2006) 216–226. https://doi.org/10.1016/j.critrevonc.2006.06.008.

[4] F. Torino, S.M. Corsello, R. Longo, et al., Hypothyroidism related to tyrosine kinase inhibitors: An emerging toxic effect of targeted therapy. *Nat. Rev. Clin. Oncol.*, 6 (2009) 219–228. https://doi.org/10.1038/nrclinonc.2009.4.

[5] N. Matsunaga, T. Kitahara, M. Yamada, et al., The influence of light sources on sunitinib measurements with photoisomerization. *Biomed. Chromatogr.*, 33 (2019). https://doi.org/10.1002/bmc.4407.

[6] J. Han, S. Zhang, J. Niu, et al., Development of taccalonolide aj-hydroxypropyl-beta-cyclodextrin inclusion complexes for treatment of clear cell renal-cell carcinoma. *Molecules*, 25 (2020). https://doi.org/10.3390/molecules25235586.

[7] G. Crini, Review: A History of Cyclodextrins. *Chem. Rev.*, 114 (2014) 10940–10975. https://doi.org/10.1021/cr500081p.

[8] G. Astray, C. Gonzalez-Barreiro, J.C. Mejuto, et al., A review on the use of cyclodextrins in foods. *Food Hydrocoll.*, 23 (2009) 1631–1640. https://doi.org/10.1016/j.foodhyd.2009.01.001.

[9] E.M.M. Del Valle, Cyclodextrins and their Uses: A Review. *Process Biochem.*, 39 (2004) 1033–1046. https://doi.org/10.1016/S0032-9592(03)00258-9.

[10] F. Fateminasab, A.K. Bordbar, B. Asadi, et al., Modified beta-cyclodextrins: Rosmarinic acid inclusion complexes as functional food ingredients show improved operations. *Food Hydrocoll.*, 131 (2022) 107731. https://doi.org/10.1016/j.foodhyd.2022.107731.

[11] T. Loftsson, D. Duchene, Cyclodextrins and their Pharmaceutical Applications. *Int. J. Pharm.*, 329 (2007) 1–11. https://doi.org/10.1016/j.ijpharm.2006.10.044.

[12] C.D. Radu, O. Parteni, L. Ochiuz, Applications of cyclodextrins in medical textiles — review. *J. Control. Release*, 224 (2016) 146–157. https://doi.org/10.1016/j.jconrel.2015.12.046.

[13] T. Loftsson, M.E. Brewster, Pharmaceutical Applications of Cyclodextrins: Basic Science and Product Development. *J. Pharm. Pharmacol.*, 62 (2010) 1607–1621. https://doi.org/10.1111/j.2042-7158.2010.01030.x.

[14] P. Mura, Advantages of the combined use of cyclodextrins and nanocarriers in drug delivery: A review. *Int. J. Pharm.*, 579 (2020) 119181. https://doi.org/10.1016/j.ijpharm.2020.119181.

[15] K. Fenyvesi, M. Vikmon, L. Szente, Cyclodextrins in Food Technology and Human Nutrition: Benefits and Limitations. *Crit. Rev. Food Sci. Nutr.*, 56 (2016) 1981–2004. https://doi.org/10.1080/10408398.2013.809513.

[16] K. Koziel, J. Lagiewka, B. Girek, et al., Synthesis of new amino-beta-cyclodextrin polymer, cross-linked with pyromellitic dianhydride and their use for the synthesis of polymeric cyclodextrin based nanoparticles. *Polymers (Basel)*, 13 (2021). https://doi.org/10.3390/polym13081332.

[17] S.R. Ignat, S. Dinescu, J. Varadi, et al., Complexation with Random Methyl-beta-Cyclodextrin and (2-Hydroxypropyl)-beta-Cyclodextrin Promotes Chrysin Effect and Potential for Liver Fibrosis Therapy. *Materials*, 13 (2020) 5003.

[18] E. Fenyvesi, J. Szeman, K. Csabai, et al., Methyl-beta-cyclodextrins: The role of number and types of substituents in solubilizing power. *J. Pharm. Sci.*, 103 (2014) 1443–1452. https://doi.org/10.1002/jps.23917.

[19] F. Fateminasab, A.K. Bordbar, S. Shityakov, et al., Comprehensive Physico-Chemical Characterization of a Serotonin Inclusion Complex with 2-Hydroxypropyl-beta-Cyclodextrin. *J. Solution Chem.*, 49 (2020) 915–944. https://doi.org/10.1007/s10953-020-00997-x.

[20] S. Tavakoli, J. Puranen, S. Bahrpeyma, et al., Liposomal sunitinib for ocular drug delivery: A potential treatment for choroidal neovascularization. *Int. J. Pharm.*, 620 (2022) 121725. https://doi.org/10.1016/j.ijpharm.2022.121725.

[21] J. He, H. Xiao, B. Li, et al., The programmed site-specific delivery of the angiostatin sunitinib and chemotherapeutic paclitaxel for highly efficient tumor treatment. *J. Mater. Chem. B*, 7 (2019) 4953–4962. https://doi.org/10.1039/c9tb01159e.

[22] Y. Wang, K. Yuan, Z. Shang, et al., Construction of nanohydrogels for enhanced delivery of hydrophilic and hydrophobic drugs and improving chemotherapy efficacy. *Eur. Polym. J.*, 186 (2023) 111838. https://doi.org/10.1016/J.EURPOLYMJ.2023.111838.

[23] J. Kralova, Z. Kejik, T. Briza, et al., Porphyrin - Cyclodextrin conjugates as a nanosystem for versatile drug delivery and multimodal cancer therapy. *J. Med. Chem.*, 53 (2010) 128–138. https://doi.org/10.1021/jm9007278.

[24] J.A. Rothwell, M. Urpi-sarda, M. Boto-ordo, et al., Systematic analysis of the polyphenol metabolome using the Phenol-Explorer database. *Mol. Nutr. Food Res.*, 60 (2016) 203–211. https://doi.org/10.1002/mnfr.201500435.

[25] S.A. Samad B., A. Hussein Al-Assady N., Preparation, characterization, and in vitro performance evaluation of polymeric scaffolds containing sodium alginate microspheres with methotrexate for controlled drug delivery. *Chem. Rev. Lett.*, 8 (2025) 829-839. https://doi.org/10.22034/crl.2024.486462.1466S

[26] M.J. Saadh, C. Hsu, R.A. Kareem, et al., Computational assessments of 5-Fluorocytosine (Flucytosine) antifungal adsorption onto a fullerene oxide nanocage for engineering a potential drug delivery platform. *Chem. Rev. Lett.*, 8 (2025) 547-554. https://doi.org/10.22034/crl.2025.512441.1561

[27] A. Abbasi, L. Edjlali, M.A. Babazadeh, et al., The development of chitosan-salicylic acid crosslinked tripolyphosphate as a pH-sensitive nanocarrier for doxorubicin-controlled release. *Chem. Rev. Lett.*, 8 (2025) 589-601. https://doi.org/10.22034/crl.2025.512140.1560

[28] L. Hokmabady, E. Mohebbi, Inclusion complexes of natural and modified cyclodextrins with nilotinib anticancer drug: insights from molecular docking and molecular dynamics simulation. *Chem. Pap.*, 79 (2025) 8799–8814. https://doi.org/10.1007/s11696-025-04352-6.

[29] F. Gholampour, L. Hokmabady, F. Ravari, Comprehensive molecular docking and molecular dynamics simulation study of unmodified and modified cyclodextrins: erlotinib inclusion complexes. *Mol. Simul.*, 50 (2024) 1515–1528. https://doi.org/10.1080/08927022.2024.2401617.

[30] E. Mohebbi, L. Hokmabady, F. Ravari, Host–guest interactions of Crizotinib with natural and modified cyclodextrins: a combined molecular docking and molecular dynamics simulation approaches. *Mol. Simul.*, 49 (2023) 1684–1697. https://doi.org/10.1080/08927022.2023.2259493.

[31] S. Kim, J. Chen, T. Cheng, et al., PubChem 2023 update. *Nucleic Acids Res.*, 51 (2023) D1373–D1380. https://doi.org/10.1093/nar/gkac956.

[32] B. Mikami, M. Hirose, Y. Morita, et al., The 2.0-A Resolution Structure of Soybean beta-Amylase complex with alpha-Cyclodextrin. *Biochemistry*, 32 (1993) 6836–6845. https://doi.org/10.1021/bi00078a006.

[33] A.K. Schmidt, S. Cottaz, H. Driguez, G.E. Schulz, Structure of cyclodextrin glycosyltransferase complex with a derivative of its main product beta-cyclodextrin. *Biochemistry*, 37 (1998) 5909–5915. https://doi.org/10.1021/bi9729918.

[34] J.C.M. Uitdehaag, K.H. Kalk, B.A. Van Der Veen, et al., The cyclization mechanism of cyclodextrin glycosyltransferase (CGTase) as revealed by a gamma-cyclodextrin-CGTase complex at 1.8-A resolution. *J. Biol. Chem.*, 274 (1999) 34868–34876. https://doi.org/10.1074/jbc.274.49.34868.

[35] H.M. Berman, J. Westbrook, Z. Feng, et al., The Protein Data Bank. *Nucleic Acids Res.*, 28 (2000) 235–242. https://doi.org/10.1038/s41577-020-00473-z.

[36] H.P. Hratchian, T.A. Keith, J. Millam, *GaussView 5 Reference*, 2009.

[37] M. Agostillo, C. Jene, T. Boyle, et al., Molecular docking of carbohydrate ligands to antibodies: Structural validation against crystal structures. *J. Chem. Inf. Model.*, 49 (2009) 2749–2760. https://doi.org/10.1021/ci900388a.

[38] D.B. Kitchen, H. Decornez, J.R. Furr, J. Bajorath, Docking and Scoring in Virtual Screening for Drug Discovery: Methods and Applications. *Nat. Rev. Drug Discov.*, 3 (2004) 935–949. https://doi.org/10.1038/nrd1549.

[39] G.M. Morris, D.S. Goodsell, R.S. Halliday, et al., Automated Docking Using a Lamarckian Genetic Algorithm and an Empirical Binding Free Energy Function. *J. Comput. Chem.*, 19 (1998) 1639–1662. https://doi.org/10.1002/jcc.20634.

[40] A.D. Bani-Yaseen, Computational molecular perspectives on the interaction of propranolol with beta-cyclodextrin in solution: Towards the drug-receptor mechanism of interaction. *J. Mol. Liq.*, 227 (2017) 280-290. https://doi.org/10.1039/c1cp20854c.

[41] J. Al-essa, D.A. Bani-Yaseen, Elucidation of the influence of tautomerization on the physicochemical stability of photoactive anticancer drug Vemurafenib in Solutions: Computational insights. *Comput. Theor. Chem.*, 1239 (2024) 114754.

[42] D. Van Der Spoel, E. Lindahl, B. Hess, et al., GROMACS: Fast, flexible, and free. *J. Comput. Chem.*, 26 (2005) 1701–1718. https://doi.org/10.1002/jcc.20291.

[43] J. Huang, A.D. Mackerell, CHARMM36 all-atom additive protein force field: Validation based on comparison to NMR data. *J. Comput. Chem.*, 34 (2013) 2135–2145. https://doi.org/10.1002/jcc.23354.

[44] K. Vanommeslaeghe, A.D. MacKerell, Automation of the CHARMM general force field (CGenFF) I: Bond perception and atom typing. *J. Chem. Inf. Model.*, 52 (2012) 3144–3154. https://doi.org/10.1021/ci300363c.

[45] S. Nose, A molecular dynamics method for simulations in the canonical ensemble. *Mol. Phys.*, 52 (1984) 255–268. http://dx.doi.org/10.1080/00268978400101201.

[46] W.G. Hoover, Canonical Dynamics—Equilibrium Phase-Space Distributions. *Phys. Rev. A*, 31 (1985) 1695–1697.

[47] M. Parrinello, A. Rahman, Polymorphic transitions in single crystals: A new molecular dynamics method. *J. Appl. Phys.*, 52 (1981) 7182–7190. https://doi.org/10.1063/1.328693.

[48] U. Essmann, L. Perera, M.L. Berkowitz, et al., A smooth particle mesh Ewald method. *J. Chem. Phys.*, 103 (1995) 8577–8593. https://doi.org/10.1063/1.470117.

[49] (a) B. Hess, H. Bekker, H.J.C. Berendsen, J.G.E.M. Fraaije, LINCS: A Linear Constraint Solver for molecular simulations. *J. Comput. Chem.*, 18 (1997) 1463–1472. https://doi.org/10.1002/(SICI)1096-987X(199709)18:12<1463::AID-JCC4>3.0.CO;2-H. (b) F. Najafi, S.S. Alamdar, E. Vaziri, Fullerene (C20) as a Sensor for the Detection of Nordazepam: DFT Simulations. *J. Med. Med. Chem.*, 1 (2025) 18–23. https://doi.org/10.22034/jmedchem.2025.526412.1004. (c) N. Mirderikvand, M. Mahboubi-Rabbani, A DFT Study on Citalopram Adsorption on the Surface of B12N12. *J. Chem. Technol.*, 1 (2025) 90–95. https://doi.org/10.22034/jchemtech.2025.538393.1015. (d) B. Mohammadi, M.R. Jalali Sarvestani, A Comparative Computational Investigation on Amantadine Adsorption on the Surfaces of Pristine, C-, Si-, and Ga-doped Aluminum Nitride Nanosheets. *J. Chem. Lett.*, 4 (2023) 66–70. https://doi.org/10.22034/jchemlett.2023.388369.1107.

[50] (a) Y. Zhao, D.G. Truhlar, The M06 suite of density functionals for main group thermochemistry, thermochemical kinetics, noncovalent interactions, excited states, and transition elements. *Theor. Chem. Acc.*, 120 (2008) 215–241. https://doi.org/10.1007/s00214-007-0310-x. (b) R. Ahmadi, Furazolidone Adsorption on the Surface of B12N12: DFT Simulations. *J. Med. Med. Chem.*, 1 (2025) 100–105. https://doi.org/10.22034/jmedchem.2025.547065.1018. (c) F. Iorhuna, A.M. Ayuba, A.T. Nyijime, Comparative study of skimmianine as an adsorptive inhibitor on Al (110) and Fe (111) crystal surface. *J. Chem. Lett.*, 4 (2023) 148–155. https://doi.org/10.22034/jchemlett.2023.398506.1117.

[51] (a) P.C. Hariharan, J.A. Pople, The influence of polarization functions on molecular orbital hydrogenation energies. *Theor. Chim. Acta*, 28 (1973) 213–222. https://doi.org/10.1007/BF00533485. (b) S.A. Vahed, Fullerene (C20) as a Sensor for Detection of Midazolam: Theoretical Insights. *J. Med. Med. Chem.*, 1 (2025) 106–110. https://doi.org/10.22034/jmedchem.2025.547513.1019. (c) T.A. Nyijime, H.F. Chahul, A.M. Ayuba, F. Iorhuna, Theoretical Study of Interaction Between Thiadiazole Derivatives on Fe(110) Surface. *J. Chem. Lett.*, 4 (2023) 86–94. https://doi.org/10.22034/jchemlett.2023.391124.1110.

[52] M.J. Frisch, et al., *Gaussian 09, Revision D.01*, Gaussian, Inc., 2013.

[53] S. Grimme, S. Ehrlich, L. Goerigk, Effect of the damping function in dispersion corrected density functional theory. *J. Comput. Chem.*, 32 (2011) 1456–1465. https://doi.org/10.1002/jcc.21759.

[54] M. Rahim, F. Madi, L. Nouar, et al., Driving forces and electronic structure in beta-cyclodextrin/3,3'-diaminodiphenylsulphone complex. *J. Mol. Liq.*, 199 (2014) 501–510. https://doi.org/10.1016/j.molliq.2014.09.035.

[55] R. Liu, X. Qin, X. Liu, et al., Host-guest interactions between oleic acid and beta-cyclodextrin: A combined experimental and theoretical study. *Food Chem.*, 387 (2022) 132910. https://doi.org/10.1016/j.foodchem.2022.132910.

[56] F. Fateminasab, A.K. Bordbar, S. Shityakov, S. Gholami, Diadzein Complexation with Unmodified Cyclodextrins: A Detailed Experimental and Theoretical Study. *J. Mol. Liq.*, 271 (2018) 80–95. https://doi.org/10.1016/j.molliq.2018.08.124.

[57] F. Fateminasab, A.K. Bordbar, S. Shityakov, Detailed chemical characterization and molecular modeling of serotonin inclusion complex with unmodified beta-cyclodextrin. *Heliyon*, 5 (2019) e01405. https://doi.org/10.1016/j.heliyon.2019.e01405.

[58] C. Cezard, X. Trivelli, F. Aubry, et al., Molecular Dynamics Studies of natural and Substituted cyclodextrins in different media. *Phys. Chem. Chem. Phys.*, 13 (2011) 15103–15121. https://doi.org/10.1039/c1cp20854c.

[59] C. Huang, C. Li, P.Y.K. Choi, et al., Effect of Cut-off Distance used in Molecular Dynamics Simulations on Fluid Properties. *Mol. Simul.*, 36 (2010) 856–864. https://doi.org/10.1080/08927022.2010.489556.

[60] J.T.S. Coimbra, R. Feghali, R.P. Ribeiro, et al., The importance of intramolecular hydrogen bonds on the translocation of the small drug piracetam through a lipid bilayer. *RSC Adv.*, 11 (2020) 899–908. https://doi.org/10.1039/d0ra09995c.

[61] W. Khuntawee, P. Wolschann, T. Rungrotmongkol, et al., Molecular Dynamics Simulations of the Interaction of Beta Cyclodextrin with Lipid Bilayer. *J. Chem. Inf. Model.*, 55 (2015). https://doi.org/10.1021/acs.jcim.5b00152.

[62] T. Yadollahi, R. Ghiasi, S. Baniyaghoob, Unveiling of interactions of ansa-titanocene dichloride and ansa-vanadocene dichloride anticancer drugs with B12N12 cage. *Inorg. Chem. Commun.*, 173 (2025) 113896. https://doi.org/10.1016/j.inoche.2025.113896

[63] R. Ghiasi, M. Nikhbakht, H. Pasdar, Interactions of the Potential Antitumor Agent Vanadocene Dichloride with C20 and M+@C20 (M= Li, Na, K) nano-cages: A DFT investigation. *Results Chem.*, 9 (2024) 101659. https://doi.org/10.1016/j.rechem.2024.101659

[64] R. Ghiasi, M. Nikbakht, A. Amiri, Understanding the Interactions between anticancer active molecules Cp2TiCl2 and Cp2VCl2 and E@Al12 (E=C, Si) cluster using Density Functional Theory Calculations. *Inorg. Chem. Commun.*, 164 (2024) 112446. https://doi.org/10.1016/j.inoche.2024.112446

[65] G. Jafari, H. Raissi, M. Shahabi, Assessment of sulfobutylether-beta-cyclodextrin as a promising Fluorometholone molecule container. *Mol. Simul.*, 48 (2022) 168–175. https://doi.org/10.1080/08927022.2021.1996575.